

Parametrisation of solar radiation at the surface under cloudless conditions and its validation against observations

Zhian Sun

Bureau of Meteorology Research Centre, Australia

Li Yunyan, Zeng Xianning and Luo Zhexian

Nanjing University of Information Sciences and Technology, Nanjing, China

Wu Jingang

Bureau of Meteorology of Jiangsu Province, China

and

Liu Jingmiao

Chinese Academy of Meteorological Sciences, Beijing, China

(Manuscript received August 2006; revised April 2007)

A parametrisation of global and net solar irradiances at the earth's surface under clear sky and aerosol-free conditions is developed based on a series of radiative transfer calculations for various atmospheric conditions that may occur in the atmosphere. Instead of parametrising the solar irradiances in a full short wave spectrum as is the common practice, the solar spectrum is divided into three bands in order to simplify the treatment of gaseous absorption. The absorption of solar radiation by water vapour, ozone and carbon dioxide in each band is processed in a manner such that the effect of their overlapping absorption is properly treated. These three species are major contributors to the greenhouse effect and are explicitly treated, while CH_4 , N_2O , and O_2 are minor contributors and their effects are implicitly considered. The solar zenith angle, surface albedo and atmospheric albedo due to Rayleigh scattering are also processed explicitly as they have a significant impact on both the global and net solar radiation. The parametrisation and the radiative transfer model are in excellent agreement. The parametrisation is also tested against observations obtained at Gaize on the Tibetan Plateau and three field research sites from the Atmospheric Radiation Measurements (ARM) program. There is good agreement at Gaize, but the errors are larger for the ARM sites, indicating the need for including aerosol effects.

Introduction

Radiative transfer is one of the most important physical processes in the atmosphere and must be treated

accurately in numerical weather prediction (NWP) and climate models. In recent decades there have been many efforts aimed at improving the accuracy of radiation measurements and modelling (for example Murcray et al. 1996; Edwards and Slingo 1996; Mlawer et al. 1997; Sun and Rikus 1999; Li and Barker 2005). Radiation is computationally time-consuming to

Corresponding author address: Z. Sun, Bureau of Meteorology Research Centre, GPO Box 1289, Melbourne, Vic. 3001, Australia.
E-mail: Z.Sun@bom.gov.au

model, and therefore its calculation in most NWP and climate models is only performed at very low frequency. The model integration time step is usually in the range 450 to 720 seconds, but the radiation frequency is often set to a two to three-hour interval. Studies (e.g. Yang and Slingo 2001) have shown that the modelled diurnal variation patterns of convection and precipitation are not in the right phase compared with observations and this may be due to the low frequency of radiation calculations. In order to improve the model simulation in the diurnal cycle, the frequency of radiation calculations should be increased to at least an hourly or half-hourly interval, but this will significantly increase the model computational burden.

Apart from the radiative heating/cooling effect in the atmosphere, the important influence of radiation on convection and precipitation is its impact on the surface processes. The radiation absorbed by the earth's surface is transformed into the sensible, latent and soil heat fluxes. If the diurnal cycle of the absorbed solar energy at the surface is not well represented in the model simulations, the sensible and latent heat flux calculations will not be correct, which in turn will influence the development of convection and precipitation. In order to improve the model surface processes, the radiation budget at the surface between the two radiation time steps should be corrected to allow for variation between radiation calculations. However, it is hard to do this by a simple interpolation because there are usually rapid changes in atmospheric conditions, especially when there are clouds present. Therefore it may be desirable to develop an appropriate method that can be used to accurately determine the surface radiation budget at a high temporal frequency (e.g. each model time step). Such an approach is used in studies of the radiation budget at the surface using satellite measurements (Gautier et al. 1980; Pinker and Ewing 1985; Li et al. 1993; Li and Leighton 1993). The global monthly mean radiation budget at the surface has been studied by several researchers using satellite measurements in conjunction with radiative transfer models (Li et al. 1995; Zhang et al. 2002). These studies have shown that the surface radiation can be accurately determined by the values measured at the top of the atmosphere together with a few other meteorological variables such as solar zenith angle, precipitable water, and cloud microphysical properties. This implies that the determination of the surface radiative budget may not require detailed estimation of all the radiative transfer processes in the atmosphere. The success of these studies implies that a similar approach may be used in a global model to determine the surface radiation budget; but these methods cannot be used directly because they depend on satellite measure-

ments. For a parametrisation, the determination of the surface radiation budget must only depend on the variables that a large-scale model can provide.

In this study, we attempt to develop such a simple scheme for the determination of solar radiation at the surface. Since the results are used in the global model they must be consistent with those determined using the full radiative transfer model. Therefore, the parametrisation is developed based on calculations using the same radiation model as employed in the global model. The work presented in this paper is focused on clear sky conditions for an aerosol-free atmosphere. The treatments of aerosols and clouds are an ongoing project and our results in these areas will be presented in the future.

Radiation model

The radiation code used is the Sun-Edwards-Slingo (SES) scheme. Originally developed by Edwards and Slingo (1996), it was modified at the Bureau of Meteorology Research Centre (BMRC) (Sun and Rikus 1999), and implemented in the BMRC Atmospheric Model (BAM) in 1997. The second version (SES2) was developed later and implemented in BAM in 2006. Compared with the first version (SES1), SES2 has undergone several advances. The number of spectral bands is increased from four to nine in the short wave to better resolve the spectral variation of Rayleigh and aerosol scattering and to better represent narrow-band absorption of trace gases. The ozone cross-section data used in SES1 are taken from Lowtran7 (Kneizys et al. 1988), which has a low spectral resolution of 100 cm^{-1} and no temperature dependence. SES2 uses new ozone cross-section data, measured by the European Space Agency (Voigt et al. 2001), which has a high spectral resolution of 5 cm^{-1} and is temperature dependent. Voigt et al. (2001) have shown that the temperature dependence of the ozone cross-section is important and should be included in the radiative transfer calculations. The absorption coefficients for other species are determined from the updated spectroscopic database HITRAN2000 (Rothman et al. 2003). The transmissions of molecular species are treated in terms of a modified correlated-k method (which will be described in a separate paper). In addition to three major absorbing species (H_2O , CO_2 and O_3) included in SES1, three extra gases (CH_4 , N_2O and O_2) are implemented in the SES2 short wave spectrum. The water vapour and oxygen continuum absorptions are also included in the SES2 short wave spectrum. The code has been extensively validated against benchmarks determined using a line-by-line radiative trans-

fer model and the error of the global downward solar radiation at the surface is less than 1 W m^{-2} . The modelled results have also been examined against observations obtained from the Atmospheric Radiation Measurements (ARM) site at Oklahoma and model errors are within 4 W m^{-2} .

Parametrisation of global solar radiation at the surface

The parametrisation is developed based on a series of calculations using the SES2 radiation model for various atmospheric conditions. The 60 levels of mid-latitude summer (MLS) atmospheric profile are used for these calculations. In order to ensure that the parametrisation can be used in a global model, the total column values of three major absorbing gases (H_2O , CO_2 , O_3) have been varied to cover all possible values occurring in the global atmosphere. Precipitable water vapour amounts are allowed to vary from 0.2 to 20 cm; ozone amounts from 100 to 500 Dobson Units (DU); and the carbon dioxide concentrations from 200 to 1000 ppmv. The impact of these changes is implemented into the radiation calculations by scaling the gaseous mixing ratio profile of the MLS atmosphere in such a way that the integrations of mixing ratios are equal to the tabled values. The effects due to N_2O , CH_4 , O_2 are also included in the calculations. Since the radiative effects of these species are relatively less important compared with the major absorbing species, the changes in mixing ratios for these minor species are not included in the parametrisation. The current values as reported in the IPCC Third Assessment (Houghton et al. 2001) are used in the full radiation calculations and the effects of these species are implicitly included in the parametrisation. The solar zenith angle and surface albedo have a significant impact on the radi-

ation at the surface and are required to be explicitly included in the parametrisation. Therefore, the solar zenith angle can vary from 0° to 90° and the surface albedo from 0 to 0.9. The Rayleigh scattering is treated explicitly and the method is described following the treatment of transmittance of the atmosphere due to molecular absorption.

After these steps, we end up with five variables required in dealing with the gaseous absorptions, mainly column-integrated concentrations of H_2O , CO_2 and O_3 , solar zenith angle and surface albedo. It is obviously difficult to consider five variables simultaneously in developing the parametrisation scheme, so to simplify the problem we use the concept of separation of variables to deal with each variable individually.

Table 1 presents the SES2 radiation band structure and absorbing species in each spectral band. It is seen that the three major species (H_2O , CO_2 , O_3) have different absorbing spectra. In the spectral bands 1-2, only ozone is included. Although there are many other absorbing species in this spectral region their effects are not included in the SES2 radiation calculations because their radiative effects are relatively small, especially at the surface. In bands 3 to 5, two species, water vapour and ozone, are included and they have overlapping absorption; in bands 6 to 9 the absorbing species are water vapour and carbon dioxide. Note that other gases in Table 1 are not required to be included explicitly as mentioned above. Based on these spectral features, we may construct three spectral bands (A, B and C) for the development of the parametrisation, as indicated in the last column of Table 1.

The use of three distinct bands for the parametrisation, as opposed to a single broadband, is expected to provide a more accurate representation of the Rayleigh scattering and gas absorption processes, both of which have a strong spectral dependence.

Table 1. Division of spectral bands of the SES radiation model (1 to 9) and major absorbing species in each band. The three bands used in the parametrisation (A, B, C) are also shown.

<i>Band</i>	<i>Spectral range (μm)</i>	<i>Species</i>	<i>Parametrisation band</i>
1	0.20~0.45	O_3	A: 0.2~0.5
2	0.45~0.50	O_3	
3	0.50~0.63	$\text{O}_3, \text{H}_2\text{O}$	B: 0.5~0.83
4	0.63~0.70	$\text{O}_3, \text{H}_2\text{O}, \text{O}_2$	
5	0.70~0.83	$\text{O}_3, \text{H}_2\text{O}, \text{O}_2$	
6	0.83~1.18	H_2O	C: 0.83~5.0
7	1.18~1.67	$\text{H}_2\text{O}, \text{CO}_2, \text{O}_2$	
8	1.67~2.50	$\text{H}_2\text{O}, \text{CO}_2, \text{CH}_4, \text{N}_2\text{O}$	
9	2.50~5.00	$\text{H}_2\text{O}, \text{CO}_2, \text{CH}_4, \text{N}_2\text{O}$	

In order to further simplify the problem, we treat the molecular absorption and scattering separately by fixing the surface albedo at zero and excluding the effect of Rayleigh scattering.

Transmittance in band A (0.2 ~ 0.5 μm)

The solar radiation absorbed by ozone is considered in this band. The solar radiation reaching the surface in this spectral region is therefore a function of total ozone amount in the atmosphere and solar zenith angle. Let the solar energy incident at the top of the atmosphere be μS_o , and the solar irradiance in this band at the surface be F_1 , where μ is the cosine of the solar zenith angle and S_o the solar constant, then the transmittance of the atmosphere due to absorption by ozone can be expressed by

$$T_1 = \frac{F_1}{\mu S_o} = f[\mu, c(O_3)] \quad \dots 1$$

where $c(O_3)$ represents the total column ozone amount in cm. In order to determine this function, we first calculate T_1 for specified ranges of μ and ozone amounts. The solar zenith angle is varied from 0 to 90° with an increment of 1° for each solar zenith angle; the total column ozone amount is varied from 100 to 500 DU with an interval of 10 DU. This results in 90 solar zenith angles and 41 total ozone amounts. We then plot T_1 against $c(O_3)/\mu$ for each value of μ , and finally fit T_1 to $c(O_3)/\mu$ in terms of an appropriate function for each μ which may best represent the relationship between T_1 and $c(O_3)$. The fitting coefficients obtained in this way are naturally a function of μ . The next step is to determine how these coefficients vary with μ and perform a numerical fit so as to better represent these variations.

Figure 1 shows the relationship between T_1 and $c(O_3)$ for three solar zenith angles (1°, 70° and 89°). It is seen that the transmittance decreases as the total ozone amount increases for a constant solar zenith angle. The best fit is found using an exponential function

$$T_1 = a_1(\mu) \exp\{b_1(\mu)c(O_3)/\mu\} \quad \dots 2$$

which is represented by the solid curves in Fig. 1.

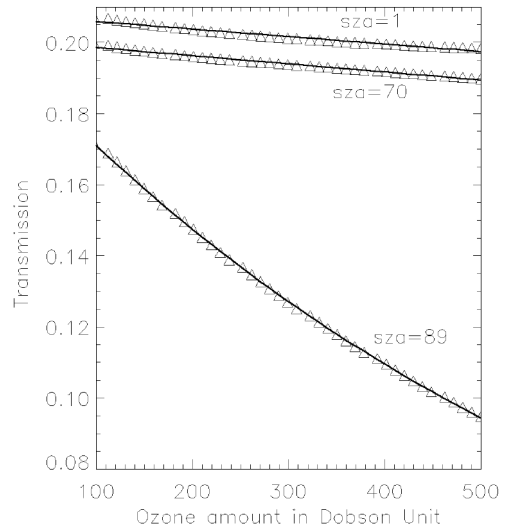
The coefficients in Eqn 2 are best represented using the following polynomial functions μ ,

$$a_1 = \sum_{i=0}^6 a_{1i} \mu^i \quad \dots 3$$

$$b_1 = \sum_{i=0}^6 b_{1i} \mu^i$$

the coefficients a_1 and b_1 are accurately reproduced for solar zenith angles between 0° and 90°. The coef-

Fig. 1 Transmittance in band A (0.2~0.5 μm) as a function of total ozone amount in Dobson Units.



ficients a_{11} and b_{11} are given in Table 2. Figure 2 shows the relationships between the coefficients and μ from the original data (symbols) and fitted results (solid curves).

The solar irradiance in spectral band A is calculated using Eqns 2 and 3 and the results are compared with those determined by the SES2 radiation model. We use the following two parameters to measure the accuracy of the parametrisation. The first is the mean relative error defined by

$$e_m = \frac{\sum_i \varepsilon_i}{\sum_i F_i(SES2)} \% \quad \dots 4$$

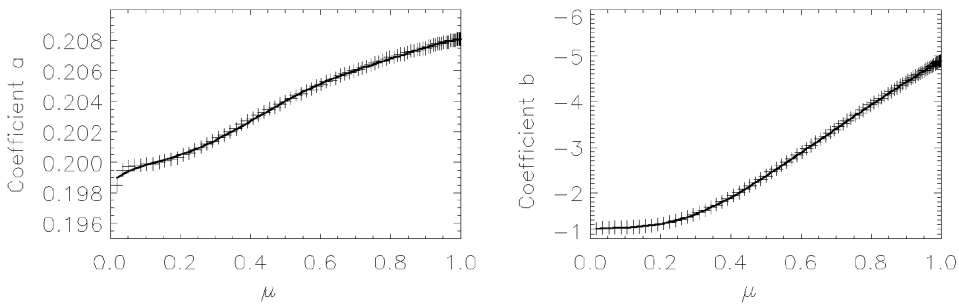
where $\varepsilon_i = |F_i(SES2) - F_i(fit)|$ is the absolute difference between solar irradiances determined by the SES2 model and the parametrisation. The second parameter is the root mean square (rms) of the error defined by

$$\sigma = \frac{1}{n} \sqrt{\sum_i [\varepsilon_i - \bar{\varepsilon}]^2} \quad \dots 5$$

where $\bar{\varepsilon}$ is the mean of ε_i . This parameter provides a measure of the range of errors. The calculations were performed for 90 solar zenith angles between 0 and 89° and 41 total ozone amounts (a total of 3690 data samples) using both the SES2 model and the parametrisation. The mean relative error of the solar irradiance in this band is only 0.18% and rms error is 0.005 W m⁻².

Table 2. Polynomial function coefficients (see Eqns 3, 10 and 14).

i	0	1	2	3	4	5	6
a_{1i}	1.99E-01	1.96E-02	-1.23E-01	5.02E-01	-8.91E-01	7.22E-01	-2.21E-01
b_{1i}	-1.21E+00	-9.35E-01	1.10E+01	-6.45E+01	1.08E+02	-7.96E+01	2.23E+01
c_{2i}	1.78E-01	2.63E+00	-1.50E+01	4.19E+01	-6.10E+01	4.44E+01	-1.27E+01
d_{2i}	-1.42E-03	-3.92E-02	1.68E-01	-3.97E-01	5.15E-01	-3.44E-01	9.24E-02
e_{2i}	3.27E+00	-5.28E+00	3.12E+01	-8.79E+01	1.28E+02	-9.26E+01	2.64E+01
f_{2i}	2.18E-05	2.86E-02	-1.32E-01	3.34E-01	-4.65E-01	3.32E-01	-9.52E-02
c_{3i}	-5.47E-02	4.87E+00	-2.48E+01	6.37E+01	-8.72E+01	6.04E+01	-1.67E+01
d_{3i}	-7.53E-01	8.44E-01	7.00E+00	-3.20E+01	5.54E+01	-4.39E+01	1.33E+01
e_{3i}	-1.91E-02	4.66E-02	-5.79E-02	2.47E-02			
f_{3i}	8.32E-03	-2.71E-02	3.57E-02	-1.54E-02			

Fig. 2 Coefficients a and b in Eqn 3 as a function of the cosine of the solar zenith angle (μ).**Transmittance in band B (0.5 ~ 0.83 μm)**

Water vapour and ozone have overlapping absorption in band B. Eqn 1 can be extended to include the effect of water vapour represented by the term W . The formula then takes the following form:

$$T_2 = f[\mu, W, c(O_3)] \quad \dots 6$$

where units for W and $c(O_3)$ are cm. In order to treat the overlapping absorption properly, a numerical fit in three steps to incorporate ozone, water vapour and solar zenith angle is performed. The procedure is similar to that for band A except that there is now an extra loop for water vapour values from 0.2 to 20 cm with an increment of 0.2 cm. This procedure leads to a series of calculations performed for 90 solar zenith angles, 41 total column ozone amounts and 100 water vapour amounts. The fitting procedure was performed as follows:

(a) For each solar zenith angle and water vapour amount, fit T_2 to ozone amounts. The following exponential function is used for this estimate:

$$T_2 = a_2(W, \mu) \exp\{b_2(W, \mu)c(O_3)/\mu\} \quad \dots 7$$

(b) For each solar zenith angle, fit the coefficients obtained from step (a) to water vapour amounts. The equations obtained are given below:

$$a_2 = c_2(\mu) \exp\{d_2(\mu)W/\mu\} \quad \dots 8$$

$$b_2 = e_2(\mu) \exp\{f_2(\mu)W/\mu\} \quad \dots 9$$

(c) Fit the coefficients obtained from step (b) to solar zenith angles. The same procedure as for band A is followed, with the solar zenith angles being fitted in terms of the polynomial functions:

$$\begin{aligned} c_2 &= \sum_{i=0}^6 c_{2i} \mu^i \\ d_2 &= \sum_{i=0}^6 d_{2i} \mu^i \\ e_2 &= \sum_{i=0}^6 e_{2i} \mu^i \\ f_2 &= \sum_{i=0}^6 f_{2i} \mu^i \end{aligned} \quad \dots 10$$

The values of the coefficients c_{2i} , d_{2i} , e_{2i} and f_{2i} are given in Table 2.

Transmittance in band C (0.83 ~ 5.0 μm)

Water vapour and carbon dioxide have overlapping absorption in this spectral region. Following the same procedures for band B, we obtained the following equations:

$$T_3 = a_3(W, \mu) + b_3(W, \mu) \log_{10}[c(\text{CO}_2)] \quad \dots 11$$

$$a_3 = c_3(\mu)(W + W^{-0.000001}) d_3(\mu) \quad \dots 12$$

$$b_3 = e_3(\mu) + f_3(\mu) \log_{10}(W + W^{-0.000001}) \quad \dots 13$$

The coefficients (c_3 , d_3 , e_3 , f_3) in Eqns 12–13 are again fitted to the cosine of the solar zenith angle in terms of the polynomial functions:

$$\begin{aligned} c_3 &= \sum_{i=0}^6 c_{3i} \mu^i \\ d_3 &= \sum_{i=0}^6 d_{3i} \mu^i \\ e_3 &= \sum_{i=0}^3 e_{3i} \mu^i \\ f_3 &= \sum_{i=0}^3 f_{3i} \mu^i \end{aligned} \quad \dots 14$$

The polynomial coefficients c_{3i} – f_{3i} are also given in Table 2. Note the unit for CO_2 in Eqn 11 is mass mixing ratio in g/g.

Rayleigh scattering albedo

We now consider the effect of Rayleigh scattering. Assuming the surface albedo is zero, then for the clear sky the atmospheric albedo of the lower atmosphere to downward-travelling irradiance (α^\uparrow) is due entirely to Rayleigh scattering. The Rayleigh scattering also increases downward-travelling irradiance by reflecting the upward-travelling irradiance back to the surface. We use α^\downarrow to represent the albedo to upward-travelling irradiance and refer to both α^\uparrow and α^\downarrow as Rayleigh scattering albedo. Lacis and Hansen (1974) developed a parametrisation of the Rayleigh albedo α^\uparrow in terms of the solar zenith angle, based on Rayleigh scattering calculations using a doubling method radiative transfer model. Although this parametrisation can be used directly in the current study, a new method may be desirable for the sake of accuracy. The effect of Rayleigh scattering depends on the total column number of atmospheric molecules. This dependency cannot be fully represented by the solar zenith angle alone. Furthermore, a constant value for α^\downarrow is assumed in the Lacis and Hansen scheme, which may not be true in the real atmosphere.

We use the surface pressure as a variable to represent the contribution to Rayleigh scattering due to different column amount of atmospheric molecules. The effect of the surface pressure is implemented into the calculations by scaling the pressure profile of the MLS atmosphere by 12 specified surface pressures ranging between 500 and 1050 hPa.

For the determination of α^\uparrow , we ran the SES2 radiation model for a Rayleigh atmosphere only, i.e. no gaseous absorptions are included and the surface albedo is set to zero. α^\uparrow is determined by

$$\alpha^\uparrow = \frac{F_0^\uparrow}{\mu S_0} \quad \dots 15$$

where F_0^\uparrow is upward irradiance at the top of the atmosphere. For estimation of α^\downarrow , the radiation model is run with the surface albedo A, and α^\downarrow is determined by

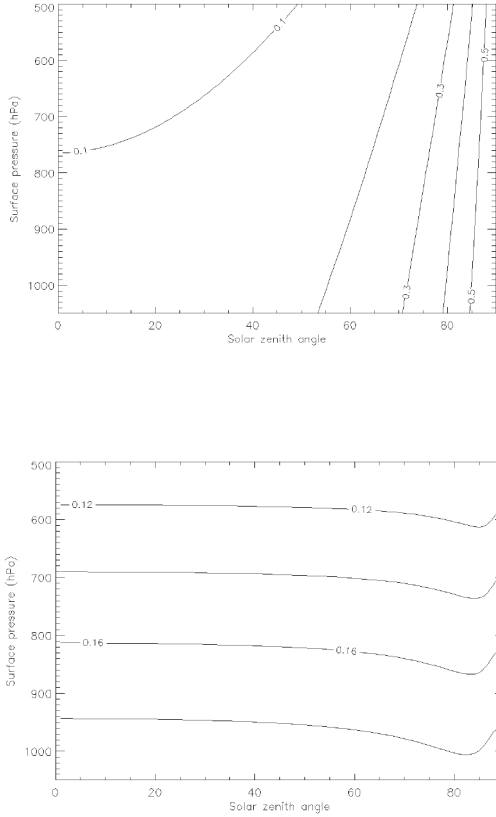
$$\alpha^\downarrow = \frac{F_A^\downarrow - F_0^\downarrow}{A F_A^\downarrow} \quad \dots 16$$

where F_A^\downarrow and F_0^\downarrow are the global solar irradiances for surface albedos of A and zero, respectively. The calculations for Rayleigh albedos were performed for 12 surface pressures, and 90 solar zenith angles from 0–89°. The calculations for Eqn 16 have been performed for several surface albedos and the results show that α^\downarrow is independent of surface albedo. A surface albedo of 0.2 was used in the analysis below.

Figure 3 shows the contour plots for both α^\uparrow and α^\downarrow for band A as a function of the solar zenith angle and surface pressure. It is seen that the albedo α^\uparrow depends strongly on the solar zenith angle and shows a relatively weak dependence on surface pressure. Although the changes of α^\uparrow with the surface pressure are smaller than those with the solar zenith angle, this effect is quite important for small solar zenith angles because the downward-travelling solar irradiance is large. For a solar zenith angle of zero, for example, α^\uparrow varies from 0.068 to 0.132 as the surface pressure changes from 500 to 1050 hPa; this leads to a difference of 64 W m^{-2} in the reflected solar irradiance if the downward-travelling solar irradiance in the lower atmosphere is 1000 W m^{-2} .

Conversely, the albedo α^\downarrow depends strongly on the surface pressure and weakly on the solar zenith angle. This is because the upward-travelling solar irradiance is completely diffuse and less dependent on the solar zenith angle. For surface pressures from 500 to 1050 hPa, α^\downarrow changes from 0.106 to 0.196. This variation causes a 9% difference in the backscattered solar irradiance at the surface, which is significant under clear sky conditions. These figures indicate that it is necessary to include effects of both the solar zenith angle and column amount of atmospheric molecules in the parametrisation of Rayleigh albedos.

Fig. 3 The Rayleigh scattering albedo as a function of the solar zenith angle and surface pressure. The upper panel shows the albedo to downward-travelling irradiance α^\downarrow ; the lower panel is the albedo to upward-travelling irradiance α^\uparrow .



The parametrisation of Rayleigh albedos is only performed in the spectral bands A and B as the Rayleigh scattering has a negligible effect in band C. The form of the parametrisation is given by

$$\begin{pmatrix} \alpha^\uparrow \\ \alpha^\downarrow \end{pmatrix} = \gamma(\mu) P_0^{\kappa(\mu)} \quad \dots 17$$

where P_0 is the surface pressure in hPa. The coefficients γ and κ are further parametrised in terms of the solar zenith angle as a polynomial function:

$$\begin{aligned} \log_{10}(\gamma) &= \sum_i \gamma_i \mu^i \\ \log_{10}(\kappa) &= \sum_i \kappa_i \mu^i \end{aligned} \quad \dots 18$$

The upper limits of summation in the above equations and the coefficients γ_i and κ_i for both α^\uparrow and α^\downarrow in bands A and B are given in Table 3.

Global and net solar radiation

Combining the effects of molecular absorption and scattering including multiple scattering between the surface and the atmosphere, the global solar irradiance at the surface for each band can be obtained by

$$F_b^\downarrow = \mu S_0 T_b (1 - \alpha^\uparrow) / (1 - A\alpha^\downarrow) \quad \dots 19$$

where T_b represents band transmittance due to absorption, $(1 - \alpha^\uparrow)$ is reflection due to Rayleigh scattering, and $(1 - A\alpha^\downarrow)$ accounts for the multiple reflection between the surface and the atmosphere. The net solar irradiance at the surface is then given by

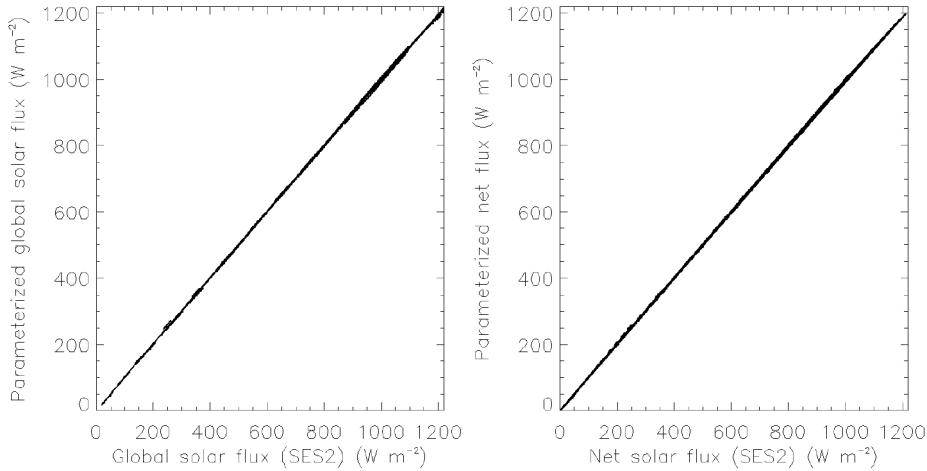
$$F_b^{net} = F_b^\downarrow (1 - A) \quad \dots 20$$

The global and net solar irradiances are determined by summing the results over the three bands. They were calculated using both the SES2 model and the parametrisation for solar zenith angles 0–90°; surface albedos 0–0.90; column amounts of water vapour 0.2–15.2 cm; column amount of ozone 100–500 Dobson Units and CO₂ mixing ratio of 200–1000 ppmv. Figure 4 shows a scatter plot of irradiance values between the SES2 model and the parametrisation. It should be emphasised that the full radiation calcu-

Table 3. Polynomial function coefficients (see Eqn 18).

α^\downarrow	band A		band B	
i	γ_i	κ_i	γ_i	κ_i
1	-3.08E+00	7.85E-01	-4.56E+00	1.01E+00
2	-9.31E+00	2.99E+00	8.29E+00	-2.76E+00
3	1.48E+02	-4.93E+01	-1.14E+02	3.92E+01
4	-1.03E+03	3.48E+02	7.62E+02	-2.65E+02
5	3.93E+03	-1.34E+03	-2.89E+03	1.01E+03
6	-9.03E+03	3.10E+03	6.67E+03	-2.34E+03
7	1.28E+04	-4.40E+03	-9.50E+03	3.34E+03
8	-1.09E+04	3.76E+03	8.17E+03	-2.88E+03
9	5.14E+03	-1.78E+03	-3.89E+03	1.37E+03
10	-1.03E+03	3.58E+02	7.86E+02	-2.78E+02
α^\uparrow	γ_i	κ_i	γ_i	κ_i
1	-3.88E-01	6.10E-02	-1.03E+00	2.60E-01
2	-1.27E+01	3.85E+00	-4.36E+01	1.18E+01
3	2.39E+01	-7.82E+00	2.94E+02	-8.56E+01
4	-2.21E+01	7.46E+00	-1.09E+03	3.25E+02
5	7.81E+00	-2.67E+00	2.27E+03	-6.85E+02
6			-2.66E+03	8.09E+02
7			1.64E+03	-5.00E+02
8			-4.11E+02	1.26E+02

Fig. 4 Comparison of global (left panel) and net (right panel) solar irradiances at the surface determined using the parametrisation with those using the SES2 radiation model.



lations with the SES2 model include all six absorbing species as shown in Table 1, and the mixing ratios of CH_4 , N_2O and O_2 are taken as their current values. It is seen that the agreement between the two schemes is excellent; the scatter points are closely distributed along the 45° diagonal line. The mean relative errors for both global and net irradiances are 0.47% and rms errors for global and net irradiances are 0.09 and 0.07 W m^{-2} , respectively. The maximum difference between the SES2 values and the corresponding parametrisation values is 17 W m^{-2} .

It should be pointed out that a simple parametrisation of the solar radiation at the surface is usually sensitive to the solar zenith angle as reported by Masuda et al. (1995) and Batlles et al. (2000). The errors in estimated solar irradiances are often large at large solar zenith angles. This deficiency does not exist in our parametrisation and the estimated solar irradiances are accurate at both large and small solar zenith angles. This indicates that the manner we have used to develop the parametrisation may be more appropriate to the real atmosphere. In addition, the use of the polynomial function to represent solar zenith angle dependency is also numerically efficient.

Comparison with observations

The results presented in the last section have shown that the parametrisation developed in this study can be used to determine the global and net solar radiation at the surface with a high accuracy relative to that determined by the full radiation model under clear sky and

aerosol-free atmospheres. It is important to further evaluate the parametrisation against observations, testing not only the accuracy of the parametrisation but the sensitivity to atmospheric aerosols as well, a process not included in the model. Therefore, the measured solar irradiances from the following sites representing four different geographic locations were used to validate the parametrisation: Gaize on the Tibetan Plateau (32.3°N , 84.06°E , 4420 m) and three ARM field research sites located at Lamont, Oklahoma (36.605°N , 97.485°W , 279 m), Barrow, Alaska (71.34°N , 156.6°W , 8 m) and Nauru Island in the tropical western Pacific (0.521°S , 166.916°E , 7.1 m).

Gaize data

A long-term observational project for the measurement of water vapour on the Tibetan Plateau has been conducted as a part of Japan-China collaboration since 1999. A Global Positioning System (GPS) receiver was installed at Gaize in the western part of the plateau and the total precipitable water vapour amount was retrieved from the GPS measurements. An automatic weather station (AWS) was also installed and started operation in October 1997 as part of the Japanese Experiment on the Asian Monsoon (Wang et al. 2004). Total downward and upward solar radiation and infrared thermal radiation are measured at five-second intervals by upward-looking and downward-looking high precision pyranometers (MS-802, EKO Instruments Trading Co. Ltd, Japan) and a precision pyrgeometer (MS-202) mounted on a 1.5 meter high horizontal platform. All of the radiation sensors are calibrated and repaired annually.

The site elevation of Gaize is 4420 m and the air mass here is only about a half of that at sea level. The aerosol optical depth in the visible spectrum is very stable and at around 0.1 (Zhang et al. 2003). The total precipitable water content is moderate during the rainy season with peaks less than 2 g cm^{-2} , and low during the dry season with values usually less than 0.5 g cm^{-2} . In addition, anticyclonic systems often dominate the region, so that cloudless days are common throughout the year. These conditions suggested that Gaize may be an ideal observational site to validate the model results under a clear sky.

The data collected in the year 2001 are used in this study. The data under clear sky conditions were sorted based on the total cloud fraction records available four times a day from the Gaize meteorological station. If the total cloud fractions at local time 0800, 1400 and 2000 are all less than 0.1 then the day is assumed clear and data during daylight hours are selected. It is obvious that some of the data selected under these conditions may be contaminated by cloud effects. The datasets were averaged to a one-hour time step to reduce random error.

ARM data

Data from one year (2005) from the three ARM sites (Lamont, Barrow and Nauru Island) were used. The data included the broadband downward and upward solar irradiances at the surface, the GPS column water vapour amount, and the fractional sky cover from the total sky imager. The radiation and fractional sky cover data are observed at a frequency of once per second and the GPS data at 30-minute intervals. There are two types of cloud cover in the fractional sky cover dataset, the percentage of opaque clouds and the percentage of thin clouds. Conditions were accepted as being cloudless when both the opaque and thin cloud percentages were less than 1%. The corresponding radiation and GPS water vapour data were then selected. Note that all ARM data used in the comparison are instantaneous observations.

Other input data

Daily total column ozone amounts are available in real time from the Total Ozone Mapping Spectrometer (TOMS, http://toms.gsfc.nasa.gov/ozone/ozone_v8.html) for a global coverage with $1^\circ \times 1.25^\circ$ latitude and longitude resolution. Data corresponding to the selected clear sky days were used in the calculations. The ozone values at all four locations were determined by linear interpolation from the TOMS data. The CO_2 mixing ratio of 375 ppm is used in the calculations and the solar constant is set to be 1368 W m^{-2} , which is the same as used in the SES2 full radiation calculation and is also a recommended

value based on satellite measurements (<http://edmall.gsfc.nasa.gov/inv99Project.Site/Pages/science-briefs/ed-stickler/ed-irradiance.html>). The sun-earth distance correction is also applied to the total solar irradiance calculations.

Results of the comparison

Figure 5 shows the scatter plots between the modelled and observed global solar radiation (left panel) and net radiation (right panel) at Gaize under clear sky conditions. It is seen that both the global and net solar irradiances determined using the parametrisation are in reasonably good agreement with the observations. The mean relative errors from Eqn 4 for the global and net solar irradiances are 4.15% and 4.19%, respectively. The rms errors from Eqn 5 are 29.14 W m^{-2} for the global irradiance and 21.38 W m^{-2} for the net irradiance. The data points are uniformly distributed along the 45° diagonal line and no systematic bias exists. These results indicate that the atmosphere at Gaize is relatively clean and the effect of the atmospheric aerosols may not be significant there.

The results for the three ARM sites are shown in Fig. 6. The agreements between the modelled and observed irradiances are also very good. The mean relative errors of global and net solar irradiances are 6.15% and 6.19% at Lamont, 7.29% and 8.03% at Barrow and 4.06% and 4.11% at Nauru Island. The corresponding rms errors are 43.3 W m^{-2} and 35.6 W m^{-2} at Lamont, 41.7 W m^{-2} and 27.2 W m^{-2} at Barrow, and 39.7 W m^{-2} and 33.0 W m^{-2} at Nauru Island. These figures indicate that the modelled errors for the ARM sites are generally larger than those at Gaize on the Tibetan Plateau. This is partially due to the fact that the Gaize data are hourly averaged results while the ARM data are instantaneous. The main reason for the large errors at the ARM sites is probably due to the neglect of atmospheric aerosols. It is very clear from Fig. 6 that systematic biases exist at all three sites with solar irradiances determined by the

Fig. 5 Comparison of global and net solar irradiances determined by the parametrisation with field observations at Gaize, Tibetan Plateau.

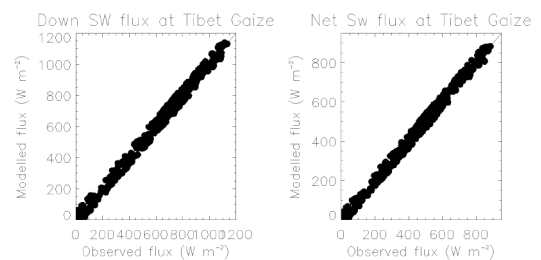
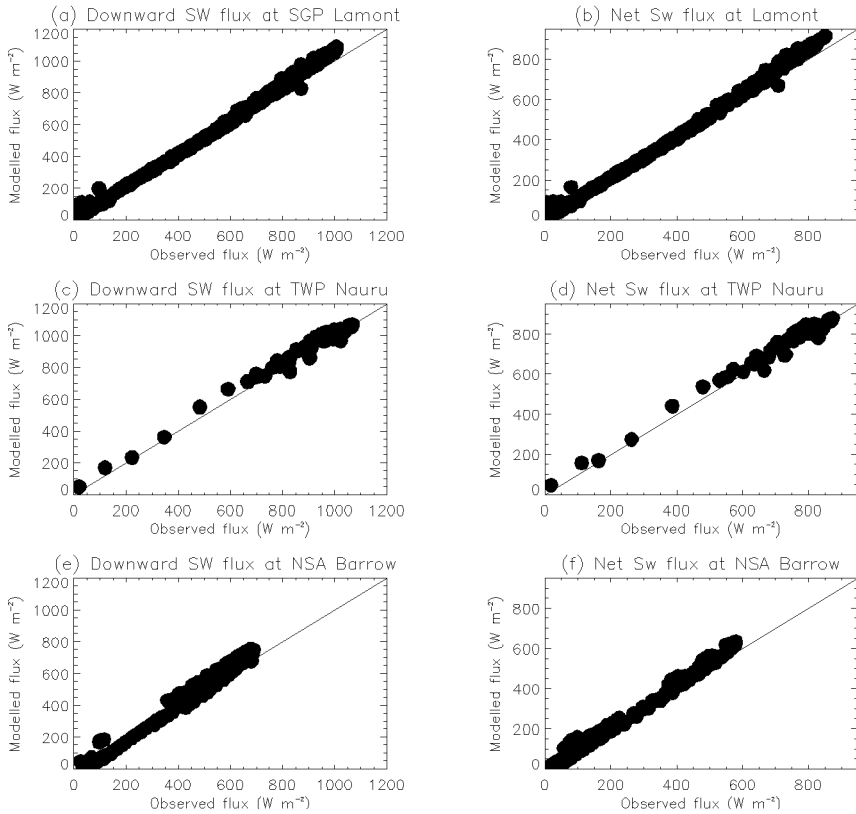


Fig. 6 Comparison of global and net solar irradiances determined by the parametrisation with field observations at three ARM sites (Lamont, Nauru Island and Barrow).



parametrisation being overestimated compared with observations. The positive biases are particularly apparent at Lamont and Barrow. These biases clearly reflect the effect of the atmospheric aerosols and indicate a necessity to include the aerosol radiative effect in the parametrisation.

Summary and discussion

A simple parametrisation scheme for calculating the global downward and net solar irradiances at the surface under clear sky and aerosol-free atmospheres has been developed. Our scheme is based on detailed radiative transfer with input variables consisting of total precipitable water vapour, ozone, carbon dioxide, solar zenith angle and surface albedo. The effects of minor trace gases are implicitly included in the scheme. The atmospheric albedo due to Rayleigh scattering is parametrised separately in terms of the solar zenith angle and surface pressure. The para-

metrisation reproduces the full radiation model calculations to a high level of accuracy. The parametrisation is also tested against the observations obtained on the Tibetan Plateau and three ARM field research sites. The results show that the parametrisation can be used to produce relatively accurate radiation estimates under clear sky conditions on the Tibetan Plateau, but systematic biases are found at the ARM sites, indicating a requirement to include the effects of atmospheric aerosols in the parametrisation.

Several earlier studies (e.g. Masuda et al. 1995; Battles et al. 2000) have shown that the parametrisation of solar radiation is sensitive to solar zenith angle and it is generally hard to obtain accurate results for a solar zenith angle greater than 85 degrees. The parametrisation developed in this study does not have this weakness. The results have shown that solar irradiances may be accurately determined without using additional conditions even at zenith angles of 89 degrees. This indicates that the use of a polynomial function to treat the effect of solar zenith angle is efficient yet accurate.

The aim of developing such a scheme is to enable calculation of the radiation budget at the surface to be performed at each model time-step in a large-scale NWP or climate model. The results presented in this study are only a first step toward this goal. The current scheme does not use aerosols as input, but neither does the SES2 model in forecasting mode. Inclusion of aerosols in a larger-scale model is very time consuming. The parametrisation developed here is fast and reliable, and will save considerable time. The model performance is quite satisfactory when compared with field measurements. This is because pyranometer calibration errors are between 3 to 5% depending on instrument quality, so the accuracy of the model is within 1 or 2% above calibration errors. Nevertheless, further study is required to include the effects of clouds and aerosols in the parametrisation. The treatment of aerosols and clouds is probably more complicated than the treatment of absorbing gases due to their high degree of variability in space and time. Aerosols in cloud-free air scatter and absorb solar radiation, altering the short wave transmission through the atmosphere and leading to a reduction of solar radiation at the surface. The radiative effects of aerosols are not well represented even in full radiation transfer models and large-scale NWP or climate models. Uncertainty in evaluation of the aerosol radiative effect is larger than that for greenhouse gases. Therefore, detailed investigations are needed for working out a way to parametrise the radiative effects of aerosols on the solar irradiances at the surface. This work, along with the treatment of clouds, is an important part of our ongoing research.

Acknowledgments

The authors wish to thank S. Voigt and J. Orphal for providing ozone cross-section data under ESA Contract 11340/95/NL/CN and DARA Project No. is 50EP9207. Dr Jingmiao Liu is supported by the National Natural Science Foundation of China under grant 40375035 and National 863 Project under grant 2002AA135360. Dr Rikus and Dr Naughton are thanked for internal reviewing and polishing of the manuscript. Dr Manuel Nunez and two anonymous referees made many valuable comments that led to significant improvement of the paper.

References

- Battles, F.J., Olmo, F.J., Tovar, J. and Alados-Arboledas, L. 2000. Comparison of cloudless sky parameterizations of solar irradiance at various Spanish midlatitude locations. *Theor. Appl. Climatol.*, 66, 81-93.
- Edwards, J.M. and Slingo, A. 1996. Studies with a flexible new radiation code. I: Choosing a configuration for a large-scale model. *Q. Jl R. Met. Soc.*, 122, 689-719.
- Gautier, C., Diak, G. and Masse, S. 1980. A simple physical model to estimate incident solar radiation at the surface from GOES satellite data. *Jnl appl. Met.*, 19, 1005-12.
- Houghton, J.T., Ding, Y., Griggs, D.J., Noguera, M., van der Linden, P.J. and Xiaosu, D. 2001. *IPCC Third Assessment Report: Climate Change 2001* (Eds.) Cambridge University Press, UK, 944 pp.
- Kneizys, F.X., Shettle, E.P., Abreu, L.W., Chetwynd, J.H., Anderson, G.P., Gallery, W.O., Selby, J.E.A. and Clough, S.A. 1988. User's guide to LOWTRAN7, *AFGL Tech. Rep. AFGL-TR-88-0177*, Air Force Geophys. Lab., Bedford, Mass.
- Lacis, A.A. and Hansen, J.E. 1974. A parameterization for the absorption of solar radiation in the Earth's atmosphere. *J. Atmos. Sci.*, 31, 118-33.
- Li, J. and Barker, H.W. 2005. A radiation algorithm with correlated-k distribution. Part I: Local thermal equilibrium. *J. Atmos. Sci.*, 62, 286-309.
- Li, Z., Charlock, T. and Whitlock, C. 1995. Assessment of the global monthly mean surface insolation estimated from satellite measurements using global energy balance archive data. *Jnl climate*, 8, 315-28.
- Li, Z., Leighton H.G., Masuda, K. and Takashima, T. 1993. Estimation of SW flux absorbed at the surface from TOA reflected flux. *Jnl climate*, 6, 317-30.
- Li, Z. and Leighton, H.G. 1993. Global climatologies of solar radiation budgets at the surface and in the atmosphere from 5 years of ERBE data. *J. Geophys. Res.*, 98, 4919-30.
- Masuda, K., Leighton, H.G. and Li, Z. 1995. A new parameterization for the determination of solar flux absorbed at the surface from satellite measurements. *Jnl climate*, 8, 1615-29.
- Mlawer, E.J., Taubman, S.J., Brown, P.D., Iacono, M.J. and Clough, S.A. 1997. Radiative transfer for inhomogeneous atmospheres: RRTM, a validated correlated-k model for the longwave. *J. Geophys. Res.*, 102, 16,663-82.
- Murcray, F., Stephen, T. and Kusters, J. 1996. Instrument development for Atmospheric Radiation Measurement (ARM): Status of the Atmospheric Emitted Radiance Interferometer-Extended Resolution (AERI-X), the solar Radiance Transmission Interferometer (SORTI), and the Absolute Solar Transmission Interferometer (ASTI). In *Proceedings of the Fifth Atmospheric Radiation Measurement (ARM) Science Team Meeting*, CONF-9503140, U.S. Department of Energy, Washington, D.C., 225-6.
- Pinker, R.T. and Ewing, J.A. 1985. Modeling surface solar radiation: model formulation and validation. *Jnl Clim. Appl. Met.*, 24, 389-401.
- Rothman, L.S., Barbe, A., Benner, D.C., Brown, L.R., Camy-Peyret, C., Carleer, M.R., Chance, K., Clerbaux, C., Dana, V., Devi, V.M., Fayt, A., Flaud, J.-M., Gamache, R.R., Goldman, A., Jacquemart, D., Jucks, K.W., Lafferty, W.J., Mandin, J.-Y., Massie, S.T., Nemtchinov, V., Newnham, D.A., Perrin, A., Rinsland, C.P., Schroeder, J., Smith, K.M., Smith, M.A.H., Tang, K., Toth, R.A., Vander Auwera, J., Varanasi, P. and Yoshino, K. 2003. The HITRAN molecular spectroscopic database: Edition of 2000 including updates of 2001. *J. Quant. Spectrosc. Rad. Transfer*, 82, 5-44.
- Sun, Z. and Rikus, L. 1999. Improved application of exponential sum fitting transmissions to inhomogeneous atmosphere. *J. Geophys. Res.*, 104, 6291-304.
- Wang, K., Liu, J., Zhou, X., Sparrow, M. and Sun, Z. 2004. Validation of the MODIS global surface albedo product using ground measurements in a semi-desert area over the Tibetan Plateau. *J. Geophys. Res.*, 109, D05107, doi: 10.1029/2003JD004229.
- Voigt, S., Orphal, J., Bogumil, K. and Burrows, J.P. 2001. The temperature dependence (203-293 K) of the absorption cross-section

- tions of O₃ in the 230-850 nm region measured by fourier-transform spectroscopy. *J. Photochem. Photobiol.*, *A143*, 1-9.
- Zhang, J.H., Si, Z.J., Mao, J.T. and Wang, M.H. 2003. Remote sensing aerosol optical depths over China using GMS-5 satellite (in Chinese). *Chin. J. Atmos. Sci.*, *27*, 23-35.
- Zhang, Y., Li, Z. and Macke, A. 2002. Retrieval of surface solar radiation budget under ice cloud sky: uncertainty analysis and parameterization. *J. Atmos. Sci.*, *59*, 2951-65.
- Yang, G.-Y. and Slingo, J.M. 2001. The diurnal cycle in the tropics. *Mon. Weath. Rev.*, *129*, 784-801.